

Entropic stabilization of large adsorbates on weakly binding substrates – a thermal desorption and scanning tunneling microscopy study

Michael Roos,^a Achim Breitruck, Harry E. Hoster,^{*a} and R. Jürgen Behm^a

Received (in XXX, XXX) Xth XXXXXXXXX 200X, Accepted Xth XXXXXXXXX 200X

First published on the web Xth XXXXXXXXX 200X

DOI: 10.1039/b000000x

Thermal desorption (TD) of oligopyridine from HOPG shifts from ~700 to ~500 K when going from (sub-)mono- to multilayers. Stabilization of low coverages results from a continuous shift of the frequency factor ν from of 10^{15} s^{-1} for submonolayers to 10^{24} s^{-1} for multilayers whereas the desorption barrier is virtually constant. Applying transition state theory (TST), we can explain this by a change from rotationally/translationally mobile, flat-lying molecules (submonolayer) to immobile, upright molecules (multilayer). At room temperature, (time resolved) scanning tunneling microscopy (STM) gives evidence for the existence and the stability of the mobile phase.

A common phenomenon in thin film growth is a distinctly higher stability of the layer(s) directly interacting with the substrate. This becomes apparent in thermal desorption experiments, where this layer desorbs at higher temperatures than higher layers. Based on the Polanyi-Wigner-equation for the desorption rate, $r_{\text{des}} = N^n \nu \exp(-E_{\text{des}}^*/RT)$, this is usually explained by a higher desorption barrier E_{des}^* , due to a stronger interaction between adsorbate and substrate in the first layer than between adsorbates in higher layers $1-3$ (N = number of adsorbates/unit area, n = kinetic order, ν = frequency factor, R = gas constant, T = temperature). As part of the increasing interest in organic films for various applications,⁴ their stability and desorption behavior was investigated in a growing number of studies.⁵⁻⁷ They revealed dramatic increases of the frequency factor ν with the size of the respective molecule.⁸⁻¹³ This was attributed to the increase in motional and internal degrees of freedom upon desorption.

For triphenylene derivatives on Au(111), a heating rate analysis of individual TD peaks recently revealed that ν can be dramatically higher for desorption from multilayer than from monolayer films.⁷ Based on TST, this trend was attributed to an immobilization of the molecules within the crystallites formed at higher coverages, which in turn increases the driving force towards desorption via entropy effects.

In the present paper, we will show that such a thickness dependent increase of ν can be tracked continuously for coverages varied over more than three orders of magnitude. This is possible by analyzing the leading edges instead of the peaks of the TD spectra.¹ Furthermore, we will demonstrate that TST in combination with coarse information about the internal molecule structure can explain the observed trend even quantitatively.

^a Institute of Surface Chemistry and Catalysis, Ulm University, D-89069 Ulm, Germany; E-mail: harry.hoster@uni-ulm.de

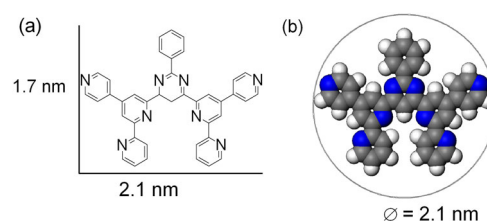


Fig. 1 (a) Schematic structure of 2,4'-BTP with lateral dimensions of 1.7 nm \times 2.1 nm. (b) 2,4'-BTP model indicating the space required for free rotation (circle).

As model system, we have chosen oligopyridine 2,4'-BTP (see Fig. 1)^{14,15} adsorbed on highly oriented pyrolytic graphite (HOPG). In that system, the molecule-substrate bonding is dominated by π - π interactions, whereas molecule-molecule interactions additionally include hydrogen bonding.^{15,16} In combination with nm-scale STM-imaging, our TD data also yield the peculiar finding that the self-assembled hydrogen bonded networks are less stable against desorption than less densely packed ones.

Desorption spectra were recorded in a UHV system equipped with a home-built evaporator, a quadrupole mass spectrometer (Pfeiffer QMA 400), and a manipulator for sample positioning and heating. The HOPG sample ($1 \times 1 \text{ cm}^2$) was glued onto a Ta sample holder, which in turn was attached to two W wires for resistive heating. Clean HOPG surfaces were prepared by tape stripping and annealing in UHV at 1000 K for > 5 min. As in previous works,^{15,16} STM images were recorded at 300 K by a home-built setup, using constant-current and constant-height mode for frame rates of 0.017 s^{-1} and 2 s^{-1} , respectively.

At a coverage of $N = 0.39 \text{ nm}^{-2}$ (molecules per nm^2), 2,4'-BTP adsorbs in a flat-lying geometry on HOPG and forms a highly ordered quasi-quadratic network (QQN).¹⁶ A typical STM image is shown in Fig. 2b.¹⁵ The highest possible coverage of planarly adsorbed 2,4'-BTP is 0.44 nm^{-2} .^{15,16} A monolayer film with QQN structure can be reproducibly prepared by excess deposition, followed by annealing at 570 K for 5 min.¹⁵ This procedure was utilized to calibrate N and r_{des} (molecules $\text{nm}^{-2} \text{ s}^{-1}$) in the thermal desorption experiments (see Fig. 2a). In the low coverage range of $N < 0.3 \text{ nm}^{-2}$, no ordered structures are visible by STM at 300 K, which we attribute to the predominance of a dilute two-dimensional gas (2DG). For $0.3 \text{ nm}^{-2} < N < 0.39 \text{ nm}^{-2}$, STM imaging reveals coexistence of QQN and 2DG. Figs 2d-2e show a sequence of images of a dynamic QQN|2DG boundary, recorded with a line frequency of 600 s^{-1} .

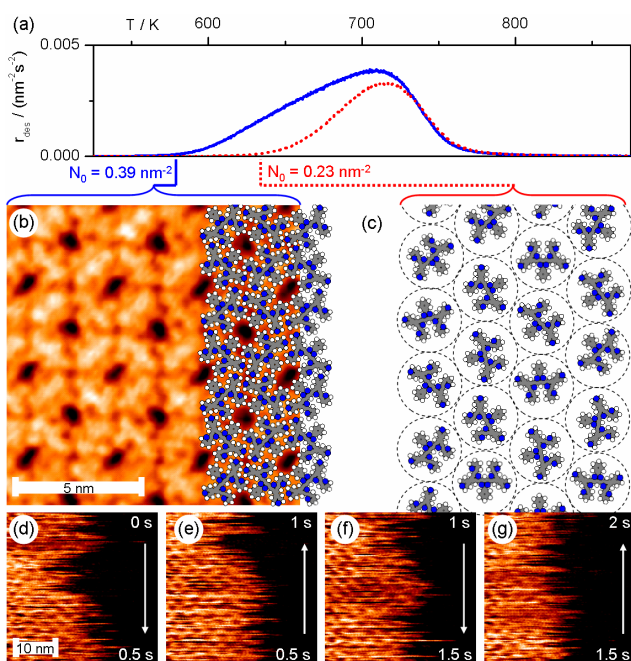


Fig. 2 (a) Thermal desorption spectra for $N_0 = 0.39 \text{ nm}^{-2}$ (QQN phase, see text) and $N_0 = 0.23 \text{ nm}^{-2}$. (b) STM image of the QQN phase ($11 \times 11 \text{ nm}^2$, 1 frame minute^{-1} , $U_T = -1.6 \text{ V}$, $I_T = 5.6 \text{ pA}$) with superimposed structure model. (c) Visualization of adlayer of rotating and mobile molecules at $N_0 = 0.23 \text{ nm}^{-2}$. (d)-(g) Sequence of STM images (2 frames s^{-1} , 300 K, $32 \times 32 \text{ nm}^2$, $U_T = -1.6 \text{ V}$, $I_T = 5.6 \text{ pA}$) at the border between QQN (left) and 2DG (right, invisible).

The left hand side shows the typical pattern of the QQN phase, whereas the 2DG region simply appears dark. The local boundary often moves by more than 5 nm from one line to the next, which means that rows of more than two molecules are locally added or removed with rates of $\sim 600 \text{ s}^{-1}$. While a more quantitative evaluation of these fluctuations will be subject of future work, their observation in combination with the absence of the hydrogen bonded QQN at low coverages indicates that the 2DG phase is the most stable phase in the low coverage regime. This is also apparent from the two TD spectra for initial coverages (N_0) of 0.39 nm^{-2} (QQN) and 0.23 nm^{-2} (2DG) compared in Fig. 2a, where the leading edge of the former starts at more than 50 K lower temperature.

As will be discussed in more detail below, the higher stability of the 2DG can be rationalized by enabled in-plane rotation and higher mobility of the molecules compared to the QQN phase. In Fig. 2c, we illustrate that the packing density of 0.23 nm^{-2} is more than low enough to allow free rotation of the single molecules and to provide a certain degree of mobility.

As apparent from Fig. 3 for TD spectra with $0.008 \leq N_0 \leq 10.43 \text{ nm}^{-2}$, the trend towards lower onset temperatures for higher N_0 can be observed over a large range of coverages (Fig. 3a: spectra with $N_0 > 1 \text{ nm}^{-2}$; Fig. 3b: all spectra, with focus on details at low N_0). The spectrum for $N_0 = 1.8 \text{ nm}^{-2}$ is marked in both diagrams, the desorption trace for $N_0 = 0.39 \text{ nm}^{-2}$ (= QQN, see also Figs. 4a and 4b) is highlighted by triangles in Fig. 3b. The spectra exhibit three distinct desorption states α , β and γ , which are successively populated with increasing N_0 . At low coverages, desorption starts at about 720 K in the γ -peak. This peak slowly shifts to lower T with higher N_0 and saturates for $N_0 \approx 0.3 \text{ nm}^{-2}$ ($T_{\text{max}} = 710 \text{ K}$). For higher N_0 , the onset of desorption shifts rapidly to lower T until $N_0 \approx 0.9 \text{ nm}^{-2}$. At this coverage, the β -peak evolves, which saturates at $N_0 \approx 1.8 \text{ nm}^{-2}$. At further increasing N_0 , the β -peak develops a low-temperature shoulder, which finally transforms into the multilayer desorption α -peak. This peak is characterized by a common leading edge and a continuous shift of T_{max} to higher temperatures, indicative of zero order desorption. With increasing coverage, only desorption rates at the low-temperature side of the spectra are increasing, supporting that the adlayers are in equilibrium. At lowest coverage, desorption occurs from the 2DG, which – based on the high desorption temperatures – is the most stable adsorbate phase. The additional desorption in the low temperature regime for $0.3 < N_0 < 0.9 \text{ nm}^{-2}$ is tentatively assigned to the completion of a planar bilayer (closest planar packing: $N_0 = 0.44 \text{ nm}^{-2}$). Saturation of the peak β at $N_0 \approx 1.8 \text{ nm}^{-2}$ would fit to the completion (i) of a 4th planar layer or (ii) of a monolayer film with the molecules in an upright orientation ('upright monolayer'), replacing the planar layers. Case (ii) would allow for a higher packing density in the first layer and would resemble the behavior of many other organic adsorbates.²

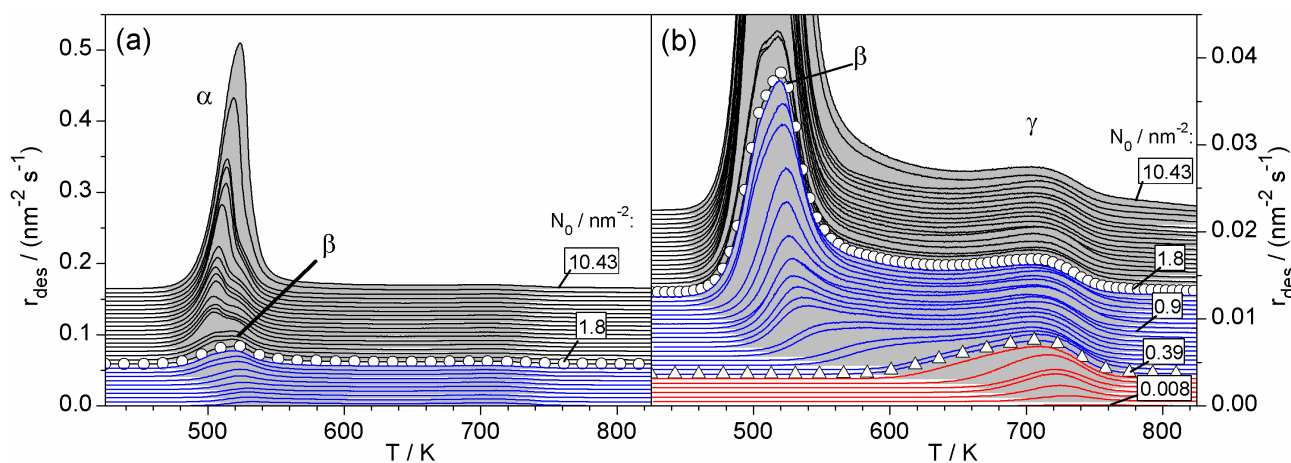


Fig. 3 TPD spectra of 2,4'-BTP molecules adsorbed on HOPG (heating rate 1.0 K s^{-1}). Initial coverages are $0.008 \leq N_0 \leq 10.43 \text{ nm}^{-2}$. (a) Overview of spectra with $N_0 > 1.0 \text{ nm}^{-2}$. (b) Enlarged view to visualize low coverage details (O) $N_0 = 1.8 \text{ nm}^{-2}$. (Δ) $N_0 = 0.39 \text{ nm}^{-2}$ (QQN phase, see text)

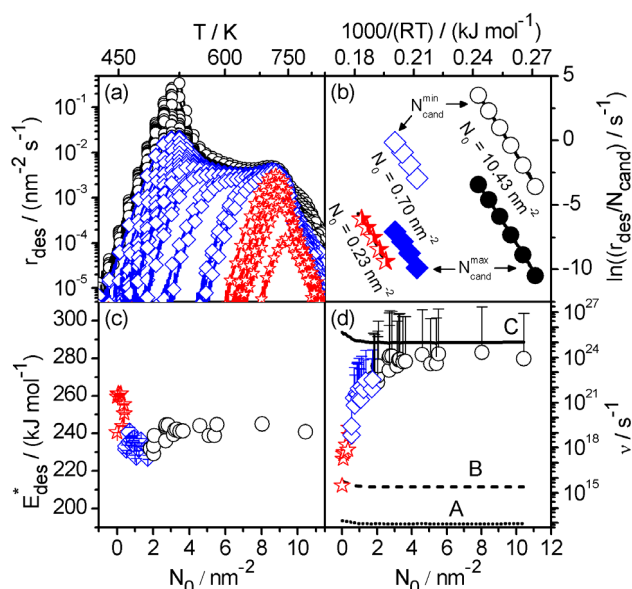


Fig. 4 (a) Menzel-Schlichting plot ($\log(r_{\text{des}})$ vs. $-1/T$), the different desorption regimes are marked by different symbols (\circ : α -peak, \square : β -peak, \star : γ -peak). (b) Arrhenius plots for three different initial coverages N_0 marked by filled ($\ln(r_{\text{des}}/N_{\text{cand}}^{\text{max}})$) and empty ($\ln(r_{\text{des}}/N_{\text{cand}}^{\text{min}})$) symbols. (c) E_{des}^* vs. N_0 and (d) v vs. N_0 derived from the slope and intercept of the Arrhenius plots. Lines A-C: TST values of v (see text).

The coverage of $N = 1.8 \text{ nm}^{-2}$ in an upright monolayer can be rationalized by a space requirement of $1.7 \times 0.33 \text{ nm}^2 = 0.56 \text{ nm}^2$ per molecule, where 0.33 nm and 1.7 nm reflect a typical π - π stacking distance⁴ and the shorter length of 2,4'-BTP molecules (see Fig. 1), respectively. Though the existence of an upright phase has to be verified by further experiments, the packing density of 1.8 nm^{-2} is a reasonable upper limit for the number of surface molecules per layer in the multilayer regime.

For analysis of the TPD data, we describe the desorption of molecules by first-order kinetics.¹¹ Zero or fractional order characteristics are considered via a coverage and structure dependent number of desorption candidates (N_{cand}). In equilibrium, the area-normalized desorption rates from different coexisting surface phases are identical,¹⁷ and possible structural effects are included in N_{cand} . The average rate can be written as $r_{\text{des}} = N_{\text{cand}} v \exp(-E_{\text{des}}^*/RT)$ or $\ln(r_{\text{des}}/N_{\text{cand}}) = \ln(v) - E_{\text{des}}^*/RT$.

For the 2DG phase of $N < 0.3 \text{ nm}^{-2}$, we set $N_{\text{cand}} = N$. For higher N , we define minimum and maximum values for the desorption candidates, $N_{\text{cand}}^{\text{min}}$ and $N_{\text{cand}}^{\text{max}}$. In the multilayer regime ($N > 1.8 \text{ nm}^{-2}$), desorption occurs predominantly from kink sites as suggested for molecular crystals.¹¹ Assuming that kink sites comprise at least 10^{-3} of all surface sites, we here set $N_{\text{cand}}^{\text{min}} = 1.8 \times 10^{-3} \text{ nm}^{-2}$ and $N_{\text{cand}}^{\text{max}} = 1.8 \text{ nm}^{-2}$. For $0.3 < N < 1.8 \text{ nm}^{-2}$, we consider the possibility of small 2D islands or 3D crystallites (3DC) with a higher fraction of edge and kink sites, and thus estimate $10^{-2} N < N_{\text{cand}} < N$.

In plots of $\ln(r_{\text{des}}/N_{\text{cand}})$ vs. $1000/(RT)$, we determined E_{des}^* and v from the slope and intercept of the desorption curves, respectively. This is illustrated for three data sets in Fig. 4b, where the lines for $r_{\text{des}}/N_{\text{cand}}^{\text{max}}$ and $r_{\text{des}}/N_{\text{cand}}^{\text{min}}$ are labeled by

superimposed solid and open symbols, respectively. E_{des}^* and v are plotted versus N_0 in Figs. 4c and 4d. Neglecting the first data point at the low coverage limit ($N_0 = 0.008 \text{ nm}^{-2}$), we obtain barriers around 260 kJ mol^{-1} for $N_0 < 0.3 \text{ nm}^{-2}$, i.e., in the range of an incomplete monolayer. For $0.3 < N_0 < 1 \text{ nm}^{-2}$, E_{des}^* decreases slightly, passes through a wide minimum around 230 kJ mol^{-1} ($1 < N_0 < 2 \text{ nm}^{-2}$), and then reaches a coverage independent value of 240 kJ mol^{-1} for $N_0 > 3 \text{ nm}^{-2}$, i.e., in the multilayer regime. We attribute these small variations of E_{des}^* at least partly, to coverage dependent structures with different hydrogen bond configurations (one H bond $\approx 10 \text{ kJ mol}^{-1}$ ¹⁵). Furthermore, structure dependent changes of $\partial v/\partial(1/T)$ ('Tolman correction'¹⁸) may mimic slight variations in the experimentally determined desorption barrier E_{des}^* , which depending on the contributions from molecular rotations on v are estimated to be in the range of 1-2 RT or 5-10 kJ mol^{-1} and thus below the variation of E_{des}^* in Fig. 4c. Compared to E_{des}^* , v exhibits a much more pronounced coverage dependence, which is plotted in Fig. 4d. Values based on $N_{\text{cand}}^{\text{max}}$ and $N_{\text{cand}}^{\text{min}}$ are marked by symbols and positive error bars, respectively. v increases from $v_{\text{min}} \approx 10^{15} \text{ s}^{-1}$ in the 2DG phase up to $v_{\text{max}} \approx 10^{24} \text{ s}^{-1}$ in the 3DC regime. It increases most steeply before the bilayer is completed at $N_0 = 0.9 \text{ nm}^{-2}$, but continues to grow for the upright phase until $N_0 \approx 3 \text{ nm}^{-2}$, where it becomes coverage independent. For the γ -peak, the values of E_{des}^* and v were also confirmed by heating rate variation experiments ($0.05 \leq \beta \leq 8.0 \text{ K s}^{-1}$) that will be published shortly. An exemplary Redhead analysis² of the peak at 720 K for $N_0 = 0.23 \text{ nm}^{-2}$ (Fig. 1a) reveals ($\beta = 1 \text{ K s}^{-1}$, $v = 10^{18} \text{ s}^{-1}$, see Fig 4d) $E_{\text{des}} = RT[\ln(720 \text{ K } v/\beta) - 3.46] = 266 \text{ kJ mol}^{-1}$, in good agreement with our leading-edge based result of 260 kJ mol^{-1} . It is obvious that, despite all uncertainties about N_{cand} , it is mainly this variation of v over nine orders of magnitude that governs the higher thermal stability of the (horizontal) monolayer compared to the upright monolayer or multilayers. This is very similar to the behavior reported for triphenylene derivatives on Au(111).⁷

The following quantitative interpretation of our results makes use of the expression $v = \frac{kT}{h} \frac{z^\ddagger}{z^{\text{ads}}}$ for the frequency

factor v in TD processes according to TST.¹⁹ k , h , z^{ads} , and z^\ddagger denote the Boltzmann and Planck constants and the molecular partition functions for the adsorbed state (AS) and the transition state (TS), respectively.^{2,10} For $T = 500 - 700 \text{ K}$, kT/h lies between 10^{13} and $1.46 \times 10^{13} \text{ s}^{-1}$, which is a typical value of v for desorption of small adsorbates. The pronounced changes of v (Fig. 4d) must therefore be due to variations of $(z^\ddagger/z^{\text{ads}})$ between 10^2 in the 2DG and 10^{11} in the multilayer regime. For desorption processes, contributions to $(z^\ddagger/z^{\text{ads}})$ mainly arise from translation, rotation, and vibration, whereas electronic excitations do not significantly change upon desorption and thus cancel.¹⁰ This means

$$\frac{r_{\text{des}}}{N_{\text{cand}}} = \frac{kT}{h} \frac{z_{\text{trans}}^\ddagger}{z_{\text{trans}}^{\text{ads}}} \frac{z_{\text{rot}}^\ddagger}{z_{\text{rot}}^{\text{ads}}} \frac{z_{\text{vib}}^\ddagger}{z_{\text{vib}}^{\text{ads}}} \cdot \exp\left(-\frac{E_{\text{des}}^*}{RT}\right).$$

The rotational partition function for a free 2,4'-BTP molecule

$$z_{rot}^{xy\ddagger} = \frac{\sqrt{\pi}}{\sigma} \left(\frac{8\pi^2 kT}{h^2} \right)^{3/2} (I_x \cdot I_y \cdot I_z)^{1/2}$$

($I_x = 1.19 \cdot 10^{-43}$, $I_y = 2.23 \cdot 10^{-43}$, $I_z = 3.43 \cdot 10^{-43}$ kg m²: moments of inertia around the x, y, z axes; $\sigma = 2$: symmetry factor). We apply this for the TS: $z_{rot}^{\ddagger} = z_{rot}^{xy\ddagger}$. For rotation about the z-

axis, as possible in the AS at low coverages, we get

$$z_{rot}^{ads} = z_{rot}^{\ddagger} = \frac{1}{\sqrt{\pi}\sigma} \left(\frac{8\pi^2 kT}{h^2} \right)^{1/2} (I_z)^{1/2} \quad (\sigma = 1).^{20}$$

Furthermore, the translational partition function for a freely moving admolecule ('particle in a box') is $z_{trans}^{2D} = A / \Lambda^2$

($\Lambda = h / \sqrt{2\pi m kT}$: thermal wavelength; A: area per molecule for lateral movement).^{2,20} Also the TS is considered as mobile in two dimensions because its third translational dimension is along the reaction coordinate and therefore skipped.¹⁹

If we assume that the properties of the TS are largely independent of the adlayer structure⁸⁻¹¹ and consequently

$z_{trans}^{\ddagger} \cdot z_{rot}^{\ddagger} \cdot z_{vib}^{\ddagger} \approx \text{const.}$, the pronounced increase of ν with coverage must be due to a decrease of the partition function of the AS, $z_{trans}^{ads} \cdot z_{rot}^{ads} \cdot z_{vib}^{ads}$, and thus of its entropy.² This trend, which reflects an increasing immobilization of the adsorbed molecules with increasing coverage, will be quantified in the

following. Assuming also z_{vib}^{ads} as largely surface structure independent, we can calculate ν by

$$\nu = \left(\frac{kT}{h} \frac{z_{vib}^{\ddagger}}{z_{vib}^{ads}} \frac{z_{trans}^{\ddagger}}{z_{trans}^{ads}} \frac{z_{rot}^{\ddagger}}{z_{rot}^{ads}} \right) \left(\frac{1}{z_{rot}^{ads} z_{trans}^{ads}} \right),$$

where only the second term varies with coverage.

To analyze trends with increasing coverage, we consider three limiting cases. (A) rotation, translation, and vibration in AS as in TS: $\nu = kT/h \approx 10^{13} \text{ s}^{-1}$. (B) adlayer of mobile and in-plane rotating molecules: $z_{trans}^{ads} = z_{trans}^{\ddagger}$ and $z_{rot}^{ads} = z_{rot}^{\ddagger}$. (C) rotation and translation frozen in the adlayer: $z_{trans}^{ads} = z_{rot}^{ads} = 1$.

(A) reflects the behavior usually observed for small adsorbates and obviously leads to too low values of ν . (B) should apply when AS $\hat{=}$ 2DG. If we tentatively set $z_{vib}^{\ddagger} = z_{vib}^{ads}$ and use $z_{rot}^{xy\ddagger} / z_{rot}^{\ddagger} = 1.53 \cdot 10^8 / 402 = 3.8 \cdot 10^5$, we get (for T = 600 K) $\nu = (kT/h) \cdot z_{rot}^{xy\ddagger} / z_{rot}^{\ddagger} = 4.8 \times 10^{18} \text{ s}^{-1}$. This is by about 10^3 larger than the value of $3.1 \times 10^{15} \text{ s}^{-1}$ observed experimentally for the

lowest initial adsorbate density $N_0 = 0.008 \text{ nm}^{-2}$. The deviation is tentatively attributed to additional contributions from soft adsorbate-substrate vibrations of the adsorbed molecules, which would lead to a situation where $z_{vib}^{ads} > z_{vib}^{\ddagger}$, and to influences of the local chemical environment, which cannot be reasonably quantified based on the existing system specific information. To rationalize trends with increasing coverage, we formally correct for the deviation between experimental and calculated value of ν at $N_0 = 0.008 \text{ nm}^{-2}$ by setting $z_{vib}^{\ddagger} / z_{vib}^{ads} = 10^{-3}$. Furthermore, we assume a fixed value for

$z_{trans}^{\ddagger} = z_{trans}^{ads} (2DG) = 125 \text{ nm}^2 \Lambda^{-2}$, assuming $A = N_0^{-1} = 0.008^{-1} \text{ nm}^2$ molecules⁻¹. Using these values in (5), we can calculate $\nu(N_0)$ for cases (A), (B), and (C). Note that the values of T used in the calculations correspond to the experimental onset temperatures for desorption at the respective N_0 . Curves (B) and (C) in Fig. 4d agree well with the experimental values of ν in the low and high coverage limit, respectively. It should

be pointed out that only B was adjusted to the experimental values, and that our simple calculations reproduce the experimentally found change by a factor 10^9 . The lower stability of the multilayer compared to the 2DG can thus be quantitatively rationalized by a reduced translational and rotational mobility of the adsorbed molecules. Within the planar monolayer, rotation becomes hindered when the space for each molecule is smaller than a circular site with $\varnothing \sim 2.1 \text{ nm}$ (see Fig. 1b) equivalent to $N = 0.26 \text{ nm}^{-2}$ (close packed discs as in Fig. 2c, where this is shown for 0.23 nm^{-2}). This way, we can explain the pronounced downshift of the leading edge in the TPD spectra for $N_0 > 0.3 \text{ nm}^{-2}$ rather well, even on a semi-quantitative scale, via a rapid decrease in z_{rot}^{ads} . A further refinement, including also changes in z_{trans}^{ads} and z_{rot}^{ads} with increasing N, requires information about the corresponding higher coverage adlayer structures that is not yet available.

From a thermodynamic point of view, our data clearly demonstrate that the (horizontal) mobile monolayer is stabilized against formation of 3D crystallites by its higher rotational and translational entropy. Assuming $S^{\ddagger} = \text{const.}$ (see above) and using $S^{\ddagger} - S^{\text{ads}}(j) = \alpha \ln(\nu_j)$ ($\nu_j = \nu$ for molecule in phase j; S^{\ddagger} and $S^{\text{ads}}(j)$ = entropies of TS and AS; $\alpha = \text{const.}$)² we obtain $S(2DG) - S(3DC) = R \ln(\nu(3DC) / \nu(2DG)) \approx R \ln(10^{24}/10^{15}) \approx 21 R = 175 \text{ J mol}^{-1} \text{ K}^{-1}$. Already at 300 K, this is equivalent to an energy difference of $ST = 52 \text{ kJ mol}^{-1}$.

Such an entropy based stabilization of the adsorbed monolayer is likely to be generic for many films of larger molecules on weakly interacting substrates (details might differ if the adsorbates are bound much more strongly or weakly to the substrate than to the surface of a multilayer). Apart from the TD behavior, it will also affect the thermodynamically preferred structures of thin films at elevated temperatures, favoring phases with higher mobilities. In particular, preferences are expected (i) for horizontal over upright adsorption within the first monolayer due to the higher contribution from the rotational mobility of flat-lying molecules²¹ and (ii) for surface wetting relative to island growth, e.g., Stranski-Krastanov over Volmer-Weber growth,²² for these systems.

Among the phases formed by flat lying adsorbates, the ordered ones may in many cases only be a "lesser evil" at higher packing densities where motion and rotation become impossible.

Acknowledgements

We thank C. Meier and U. Ziener for providing the 2,4'-BTP material. We are grateful for fruitful discussions with K. Fichthorn and J. Laskin. This work was supported by the Deutsche Forschungsgemeinschaft (SFB 569).

References

1. H. Schlichting and D. Menzel, *Surf. Sci.*, 1992, **272**, 27.
2. K. W. Kolasinski, *Surface Science*, Wiley & Sons, Chichester, 2002.
3. K. J. Schmidt and K. Christmann, *Surf. Sci.*, 2001, **492**, 167.
4. S. R. Forrest, *Chem. Rev.*, 1997, **97**, 1793.
5. R. Zacharia, H. Ulbricht, and T. Hertel, *Phys. Rev. B*, 2004, **69**, 155406.
6. Th. Wagner, H. Karacuban, A. Bannani, C. Bobisch, and R. Möller, *J. Phys. : Conference Series*, 2008, **100**, 052068.

-
7. P. Frank, N. Koch, M. Koini, R. Rieger, K. Müllen, R. Resel, and A. Winkler, *Chem. Phys. Lett.*, 2009, **473**, 321.
 8. K. Fichthorn and R. A. Miron, *Phys. Rev. Lett.*, 2002, **89**, 196103-1.
 9. S. L. Tait, Z. Dohnalek, C. T. Campbell, and B. D. Kay, *J. Chem. Phys.*, 2005, **122**, 164708.
 10. V. P. Zhdanov, *Surf. Sci. Rept.*, 1991, **12**, 186.
 11. A. Maiti, L. A. Zepeda-Ruiz, R. H. Gee, and A. K. Bunnham, *J. Phys. Chem. B*, 2007, **111**, 14290.
 12. K. R. Paserba and A. J. Gellmann, *Phys. Rev. Lett.*, 2001, **86**, 4338.
 13. L. W. Bruch, R. H. Diehl, and J. A. Venables, *Rev. Mod. Phys.*, 2007, **79**, 1381.
 14. U. Ziener, J. M. Lehn, A. Mourran, and M. Möller, *Chem. Eur. J.*, 2002, **8**, 951.
 15. H. E. Hoster, M. Roos, A. Breittruck, C. Meier, K. Tonigold, T. Waldmann, U. Ziener, and R. J. Behm, *Langmuir*, 2007, **23**, 11570.
 16. M. Roos, H. E. Hoster, A. Breittruck, and R. J. Behm, *Phys. Chem. Chem. Phys.*, 2007, **9**, 5672.
 17. H. Asada and M. Masuda, *Surf. Sci.*, 1989, **207**, 517.
 18. J. Laskin and J. H. Futrell, *J. Phys. Chem. A*, 2003, **107**, 5836.
 19. K. J. Laidler, S. Glasstone, and H. Eyring, *J. Chem. Phys.*, 1940, **8**, 659.
 20. A. Clark, *The Theory of Adsorption and Catalysis*, Academic Press, New York and London, 1970.
 21. T. Kataoka, H. Fukagawa, S. Hosoumi, K. Nebashi, K. Sakamoto, and N. Ueno, *Chem. Phys. Lett.*, 2008, **451**, 43.
 22. G. Witte, K. Hänel, S. Söhnchen, and Ch. Wöll, *Appl. Phys. A*, 2006, **82**, 447.